COBEM 2021 26th International Congress of Mechanical Engineering
November 22-26, 2021, Virtual Congress, Brazil
ABCM Associação Brasileira de Engenharia e Ciências Mecânicas

COB-2021-1467
FLOW VISUALIZATION IN AIRFOILS WITH PROTUBERANCES ON THE LEADING EDGE BY CFD-*OPENFOAM®*

Daniel Barbosa Barconi[1]
Aluisio Viais Pantaleão[2]
São Paulo State University, School of Engineering, Department of Mechanical Engineering, 15385-000, Ilha Solteira, SP, Brazil
[1]daniel.barconi@unesp.br
[2]aluisio.pantaleao@unesp.br

Abstract. *One of the main applications of computational fluid dynamics, which have been used in several engineering fields since the end of the 20th century, is the understanding of phenomena linked to vehicular hydrodynamics and aerodynamics, especially those related to increased performance of hydrofoils, airfoils and wings through passives devices inserted on the surface of these bodies. Thus, in the present work, a methodology was developed using CFD (Computational Fluid Dynamics) techniques to investigate and understand the hydrodynamics of Humpback whale fin-inspired airfoils, in which protuberances located on the leading edge possibly promote performance improvement. For this study, four different types of leading edge protuberances were projected on a NACA* 63_4*-021 baseline profile through a 3D-CAD open-source software. Using the* $OpenFOAM^{®}$ *platform, transient numerical simulations were performed to record the flow topology for different Reynolds numbers, angles of attack, and types of protuberance. Qualitative results obtained for stream lines, detachment point and vortex generation were compared with flow visualization photographs taken in previous experimental work found in the literature, in order to evaluate the numerical simulation. Numerical results obtained using the* k*-*ω SST *turbulent model, within a pertinent Reynolds number range, were expected to be close to the flow topology reported by experimental literature. In fact, there was good agreement between numerical and experimental qualitative results. Using aerodynamics concepts, these results allowed to infer and indicate improved performance by the modified airfoils, to the extent that there were certain disagreements between the flow detachment points of baseline profiles and those with leading edge protuberances. Such disagreements actually corresponded to flow detachment point delays, which may indicate lift gains. In this sense, for an an angle and attack of* 2^o *and at* 1900 *Reynolds number, it were obtained numerical results suggesting lift gains by the* $4S$*,* $8S$ *and* $8M$ *airfoils. Further studies are being developed to evaluate the implementation of modified airfoils in engineering applications, such as hydraulic turbines.*

Keywords: *CFD,* $OpenFOAM^{®}$*, Humpback whale fins, Lift gains*

1. INTRODUCTION

Natural selection is responsible for the morphology of all species found in nature. In this way, a mutation can represent an adaptive advantage for a living being, which, when surviving, transmits its new characteristic to subsequent generations Darwin (1859). Based on this premise, several engineering solutions can arise from the current morphology of living beings, which is the result of billions of years of natural evolution. In this context, humpback whale fins have been studied in scientific works over the last decades, due to their peculiar protuberances located on the leading edge that may represent an adaptive advantage of this species.

The characteristics and geometric parameters of humpback whale fins were first described by Fish and Battle (1995). In their work, authors set the NACA 63_4-021 profile as a representative cross-section of the humpback whale's fins. Subsequently, through experimental tests in a hydrodynamic tunnel and using the results obtained by Fish and Battle (1995), performance enhancement of modified airfoils with different types of protuberance on the leading edge was noticed by Johari *et al.* (2007). Van Nierop *et al.* (2008) developed a mathematical model to explain the mechanisms that provide the enhanced characteristics of modified airfoils. They proposed that the protuberances altered the pressure distribution on the wing such that the separation of the boundary layer was delayed behind the peaks and this phenomena lead to a gradual onset of stall and larger stall angle.

Hansen *et al.* (2009), Chen *et al.* (2012) and Paula *et al.* (2016) also described experiments using airfoils similar to that found on humpback whale flippers, all analyzing Reynolds number in the order of 10^4 to 10^5. In their work, Hansen *et al.* (2009) noticed that the most beneficial tubercles configuration proved to be those with the smallest amplitude and narrowest wavelength for the NACA 0021 airfoil. On the other hand, results presented by Chen *et al.* (2012) indicated a very clear stall-delay phenomenon caused by tubercles on a NACA 0012 airfoil with an aspect ratio equal to 1. In this case, they also reported that the airfoil with protuberances on leading edge had no significant increase in lift, but the drag

was reduced. Paula *et al.* (2016), in turn, studied leading edge protuberances on NACA 0012 and NACA 0020 profiles, in which they observed that the increase in airfoil thickness causes aerodynamic deterioration at pre-stall regime for wavy leading edge airfoils. Simultaneously, Wei *et al.* (2015) carried out experimental work at a Reynolds number of 1.4×10^4 in which they noticed that the tubercles behave like small delta-wings, where a counter-rotating vortex pair is formed over each tubercle on a NACA 63_4-021 profile. Thus, Wei *et al.* (2015) observed that the flow separate rather easily from the baseline hydrofoil surface. Posteriorly, in their experimental and numerical studies, Hansen *et al.* (2016) have identified the presence of the tubercles on a NACA 0021 foil leads to an increased flow velocity along the trough, and a larger adverse pressure gradient, which, in turn, causes boundary-layer separation to occur in the trough at a low angle of attack at a Reynolds number of 2230.

In sequence, a numerical study performed by Rostamzadeh *et al.* (2017) indicates that in contrast to the transitional flow regime, where the unmodified NACA-0021 undergoes a sudden loss of lift, in the turbulent regime, the baseline foil experiences gradual stall and produces more lift than the tubercled foil. Also to a NACA-0021 profile and in numerical terms, using a Reynolds number of 1.2×10^5 and a $20°$ angle of attack, Perez Torro and Kim (2017) confirmed an increase in lift and reduction in drag, which they attributed to three major events: (i) the appearance of large low-pressure zone near the leading edge created by the laminar separation bubbles (LSBs); (ii) the reattachment of flow behind the LSBs resulting in a decreased volume of the rear wake; and, (iii) the deterioration of von-Kármán (periodic) vortex shedding due to the breakdown of spanwise coherent structures.

Recently, Bocalon *et al.* (2019) performed an experimental study using a vertical hydrodynamic tunnel to investigate the changes in the separation point position considering the troughs and peaks caused by the pressure gradient observed first by Hansen *et al.* (2016). In their work, three airfoils of those reported by Johari *et al.* (2007) were evaluated, as shown in Fig.1a. Bocalon *et al.* (2019) reported that the $4S$ airfoil is the one with the highest lift coefficient, in comparison with baseline and $4M$ airfoils. This conclusion was possible due to results obtained for the distance of flow detachment point from the stagnation point for each airfoil analyzed.

(a) *Baseline*, $4S$ and $4M$ geometries.

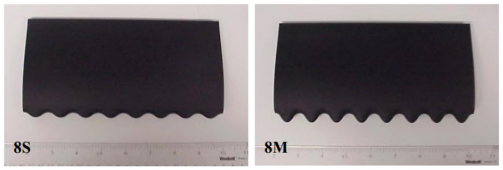

(b) $8S$ and $8M$ geometries.

Figure 1: Airfoils reported by Johari *et al.* (2007).

Therefore, the present work aims to numerically reproduce the same flow configurations in the same airfoils studied by Bocalon *et al.* (2019), in order to complement their experimental results and create numerical evidence capable to corroborate or confront their conclusions about the performance of the modified airfoils. Furthermore, in this work it was studied the behavior of two more modified airfoils, i.e., $8S$ and $8M$, also reported by Johari *et al.* (2007) and shown by Fig. 1b. Computational Fluid Dynamics (CFD) techniques were implemented to characterize the flow topology around the foils, exploring Reynolds numbers of 1400 and 1900.

2. MATERIALS AND METHODS

2.1 Computational resources

This research was carried out with the infrastructure provided by the Computational Support Center of Mechanical Engineering of the São Paulo State University (UNESP). To obtain the final results, from the initial steps of adjustment until obtaining the most adequate parameters for each simulation, it was necessary to supply a computational demand corresponding to 45 cases executed with 16 CPU's, in which according to the stage of the study the simulation time varied from 4 to 20 hours. Subsequently, additional resources were provided by the Scientific Computing Center (NCC/GridUNESP), which supplied a computational demand corresponding to 25 complementary cases executed with 48 CPU's and a simulation time varying from 3 to 6 hours.

2.2 The airfoils

The airfoils studied in this work were made through the open-source software for 3D CAD, SALOME. Therefore, as reported by Johari *et al.* (2007), the NACA 63_4-021 profile was used as baseline and the modified airfoils were designed according to the specifications shown in Tab.1.

Table 1: Geometric parameters of the modified airfoils as function of its aerodynamic chord, as reported by Johari *et al.* (2007).

Airfoil	Amplitude	Wave Lengh
4S	0.025 c	0.050 c
4M	0.50 c	0.050 c
8S	0.025 c	0.025 c
8M	0.50 c	0.025 c

Each airfoil had its width defined at $146\ mm$, respecting the lateral length of the square test section of the hydrodynamic tunnel used by Bocalon *et al.* (2019) in their experimental work. The mean chord of the airfoils was set at $70\ mm$, but the profiles trailing edge were truncated at $5\ mm$ in order to avoid problems during mesh generation. The studied airfoils geometry are shown in Fig.2

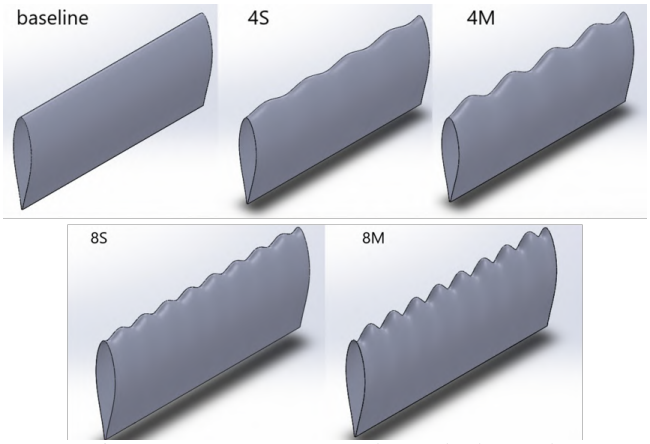

Figure 2: *3D geometry of the studied airfoils*

The airfoils shown in Fig. 2 were tilted at 2^o and 8^o to perform the simulations.

2.3 Computational procedures

2.3.1 Mesh generation

The results of this work were obtained through the implementation of the finite volume method, respecting all relevant theoretical elements related to this area of knowledge, minutely presented by Versteeg and Malalasekera (2007), Moukalled *et al.* (2016) and Maliska (2017). For this purpose, tools available in the open-source software packages based on $OpenFOAM$® were adopted, in such extent that, the spatial discretization around the airfoils was done using the $snappyHexMesh$ tool, a native dominant hexahedral mesh generator. The handling of all computational tools used in this study was carried out following the appropriate procedures well consolidated in the literature of the area and available in $OpenFOAM$® (2011). For the time discretization it was adopted a step of 0.005 seconds ranging from 0 to 45 seconds.

The mesh sensitivity analysis was based on Richardson Extrapolation (RE), i. e., the recommended method by the literature to estimate discretization errors. Since its presentation by its originator, Richardson (1911) and Richardson and Gaunt (1927), the RE has been studied and widely investigated by many authors, of which it is possible to cite Roache (1993), Ferziger and PERIĆ (1996), Broadhead *et al.* (2004) and Eça *et al.* (2007). Therefore, it was implemented the Grid Convergence Index (GCI) criterion, based on RE and presented by Celik *et al.* (2008), to find the mesh parameters corresponding to a suitable mesh size. Analyzing three meshes with 2.20, $0,74$ and 0.33 million of elements, $GCI^{32}_{coarse} = -0,001\%$ and $GCI^{32}_{fine} = 0,07\%$ it were obtained. Based on these values, it was safely adopted the 0.74 million elements mesh to obtain the numerical results of this work. Fig. 3 illustrates the meshes submitted to the described sensitivity analysis.

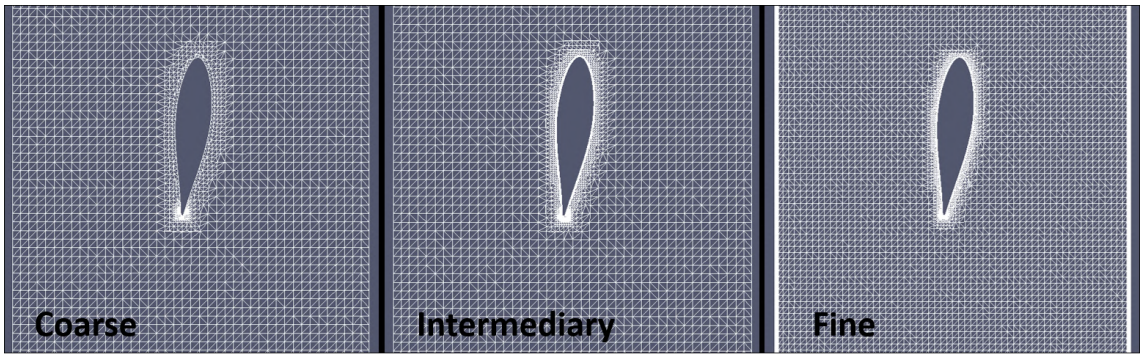

Figure 3: Meshes of 0.33, $0,74$ and 2.20 million elements.

2.3.2 Turbulence model

The k-ω SST was chosen to be implemented in this work due to its high capacity to simulate adverse pressure gradient conditions as well as flow separation when compared to other available models. Developed by Menter (1994), it is an accurate and robust method to evaluate the flow close to the wall and it also corresponds to the most widely used turbulence model in engineering applications.

However, to implement the k-ω SST turbulence model, it was necessary to refine the original mesh in order to capture the physical phenomena linked to the flow boundary layer. Proper changes in the mesh parameters raise the number of elements to 0.92 million. Due to the proximity of the results obtained for the 0.74 and 2.20 million elements meshes, it was considered that the new mesh met the GCI criterion. Thus, Fig. 4 illustrates the longitudinal section view of the final mesh generated to produce the numerical results of this work.

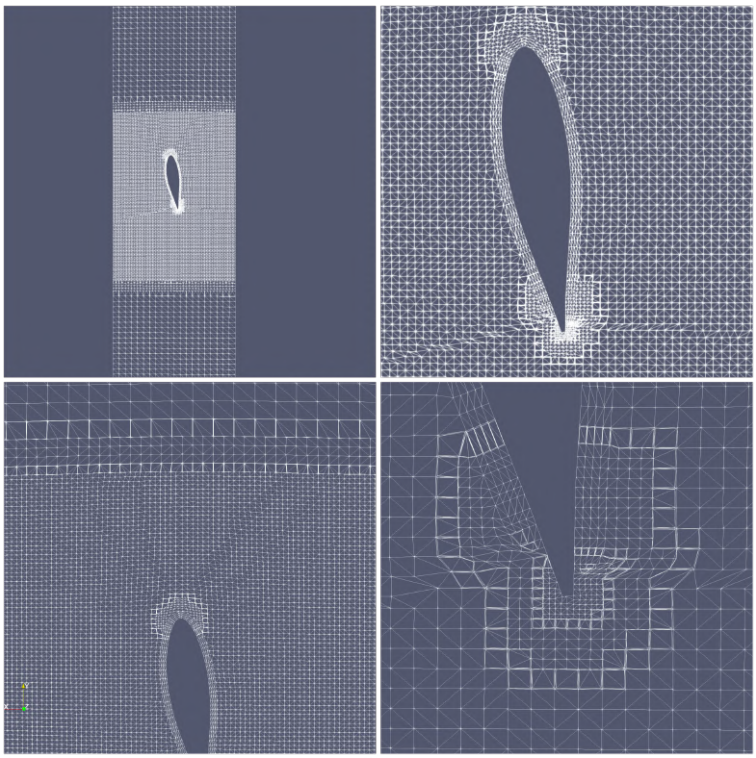

Figure 4: Section views of the final mesh topology with 0.92 million obtained through $snappyHexMesh$.

It is noteworthy that the size of the first element of the mesh shown in Fig. 4 was defined so as to meet the y^+ criterion of the turbulence model, obtaining $y^+ \leq 1$.

2.3.3 Flow conditions and numerical solver

Once the ideal mesh parameters were obtained, flows at Reynolds numbers of 1400 and 1900 were computationally simulated. Considering the average chord of the airfoils equal to 65 mm and the properties of water at Normal Tempera-

ture and Pressure (NTP) conditions, the initial flow velocities equal to 0,022 m/s and 0,029 m/s were defined in the entire computational domain to reach the respective Reynolds numbers. Boundary and initial condition to pressure, turbulent kinetic energy (k) and specific dissipation (ω) were defined following recommendations found in $OpenFOAM^{®}$ (2011).

As with any CFD problem, the main objective of this work was to numerically solve the governing equations of fluid flow and all pertinent issues involving pressure-velocity coupling. To do so, it was implemented the $pimpleFoam$ solver. The $PIMPLE$ method is a hybrid of two others, i.e., $SIMPLE$ and $PISO$ algorithms, in which the first one is formulated for purely stationary and the second one for transient problems. Detailed descriptionS of SIMPLE, PISO and PIMPLE algorithms can be found respectively in Patankar and Spalding (1983), Issa (1986) and Barton (1998).

2.3.4 Flow visualization

Graphic results were obtained through post-processing using both the open software $paraView$ and the predefined functions identified in the $OpenFOAM^{®}$ code, such as $run\text{-}time\ postprocessing$, aided by graphic interpreters, also open-sources. Thus, it were captured images of the flow corresponding to longitudinal sections at the peaks and troughs of the modified airfoils. To the baseline airfoils it were captured images of the central longitudinal sections.

After being captured, the images were handled by the open-source software *LibreOffice Impress* and it was manually measured the distance between the flow detachment point to the airfoils leading edge. Thus, dividing this values by the length of the aerodynamic chord, it was obtained the quantitative numerical results used for comparison with the experimental results presented by Bocalon *et al.* (2019).

3. RESULTS AND CONCLUSION

Once the velocity field (**u**) around each airfoil was resolved, graphical results were produced representing the vorticity (ζ) of the flow. This quantity is defined by the rotational of the velocity field, as shown in Eq. 1.

$$\zeta = \vec{\nabla} \times \mathbf{u} \tag{1}$$

Therefore, the vorticity fields obtained around each airfoils inclined in 2^o and 8^o at Reynolds numbers of 1400 and 1900 are shown in Fig.5, Fig.6 and Fig.7.

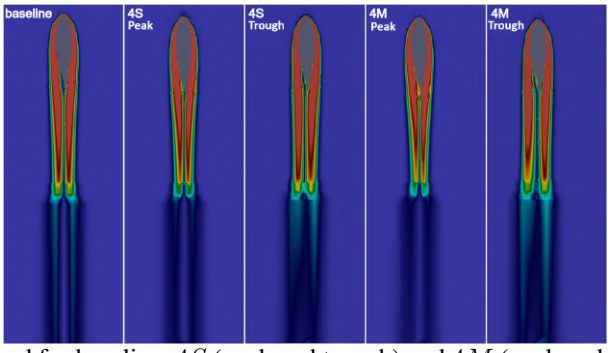

Figure 5: Vorticity results obtained for baseline, $4S$ (peak and trough) and $4M$ (peak and trough) with airfoils tilted by 2^o at 1900 Reynolds number.

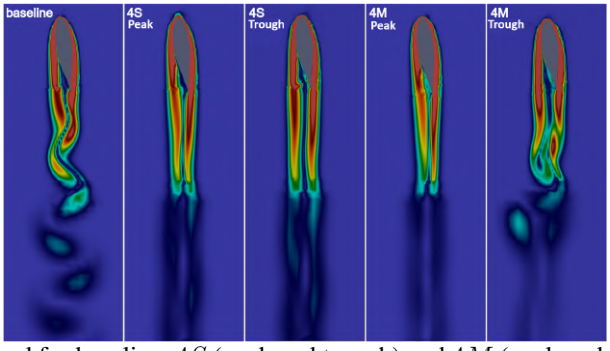

Figure 6: Vorticity results obtained for baseline, $4S$ (peak and trough) and $4M$ (peak and trough) with airfoils tilted by 8^o at 1400 Reynolds number.

The obtained flows topology were qualitatively close to the experimental visualizations carried out by Bocalon *et al.* (2019). In fact, for 1900 Reynolds number and 2^o of inclination, it was not observed numerically the generation of

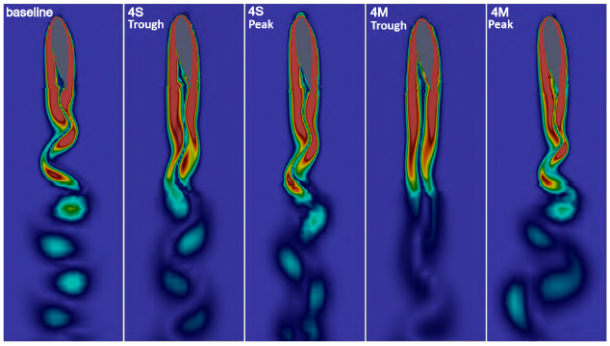

Figure 7: Vorticity results obtained for baseline, $4S$ (peak and trough) and $4M$ (peak and trough) with airfoils tilted by 8^o at 1900 Reynolds number.

vortexes with the same intensity as reported by Bocalon *et al.* (2019). However, considerable qualitative similarities lies in the length of the vortex trail and in the relative position of the detachment point to the profiles leading edge. By way of example, the experimental flow visualization by Bocalon *et al.* (2019) for 1900 Reynolds number and 8^o of attack angle is show in Fig. 8.

Figure 8: Flow topology obtained by Bocalon *et al.* (2019) for baseline, $4S$ and $4M$ airfoils at 1900 Reynolds number and 8^o of attack angle

In a complementary way, the vorticity fields obtained around the $8S$ and $8M$ airfoils are shown in Fig.9, Fig.10 and Fig.11.

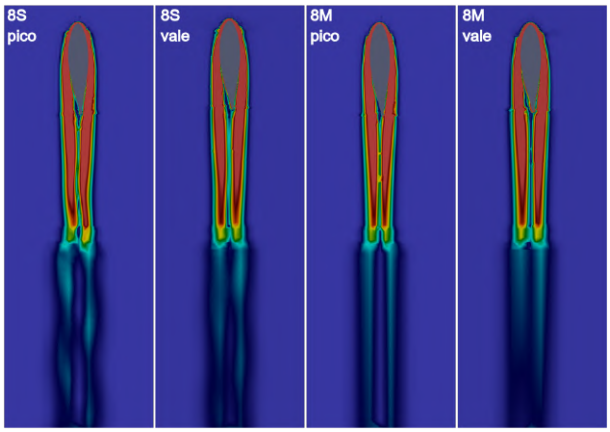

Figure 9: Vorticity results obtained for $8S$ (peak and trough) and $8M$ (peak and trough) with airfoils tilted by 2^o at 1900 Reynolds number.

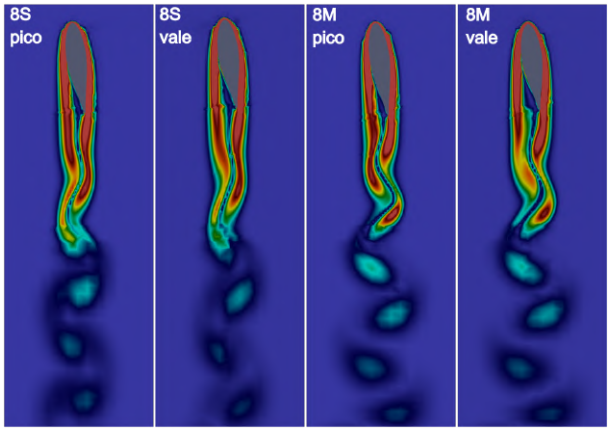

Figure 10: Vorticity results obtained for $8S$ (peak and trough) and $8M$ (peak and trough) with airfoils tilted by 8^o at 1400 Reynolds number.

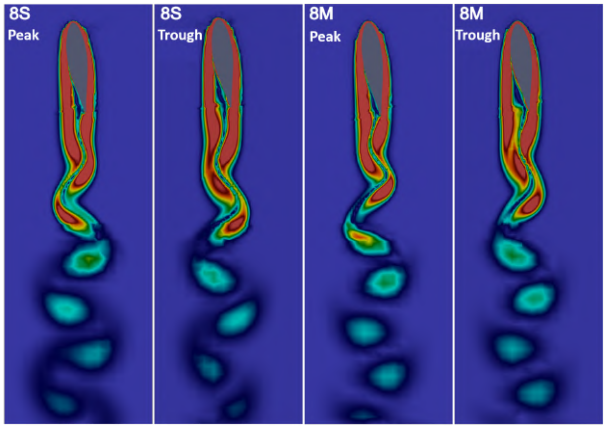

Figure 11: Vorticity results obtained for $8S$ (peak and trough) and $8M$ (peak and trough) with airfoils tilted by 8^o at 1900 Reynolds number.

Following the procedures described in Section 2, it were obtained the distances between the detachment point and the leading edge of each profile in percentage of its aerodynamic chord, as shown in Tab. 2

Table 2: Numerically obtained distance between the detachment point and the airfoils leading edges in percentage of aerodynamic chord.

α	*Re*	Baseline (%)	4S-peak (%)	4S-trough (%)	4M-peak (%)	4M-trough (%)
2^o	1900	70.2	77.3	75.1	78.7	68.3
8^o	1400	59.8	61.9	56.2	64.4	49.9
8^o	1900	64.0	65.4	57.9	66.6	54.8

Tab. 3, in turn, presents the corresponding experimental results obtained by Bocalon *et al.* (2019). Tab. 4, on the other hand, presents the analogous results obtained for the $8S$ and $8M$ airfoils.

Table 3: Distance between the detachment point and the airfoils leading edges in percentage of aerodynamic chord experimentally obtained by Bocalon *et al.* (2019).

α	*Re*	Baseline (%)	4S-peak (%)	4S-trough (%)	4M-peak (%)	4M-trough (%)
2^o	1900	68.0	72.0	73.0	78.7	67.0
8^o	1400	46.9	78.7	63.0	78.4	53.5
8^o	1900	67.6	79.4	59.3	72.0	68.4

Table 4: Numerically obtained distance between the detachment point and the $8S$ and $8M$ airfoils leading edges in percentage of aerodynamic chord

α	*Re*	8S-peak (%)	8S-trough (%)	8M-peak (%)	8M-trough (%)
2^o	1900	75.8	70.4	78.5	77.0
8^o	1400	64.5	57.8	65.8	53.2
8^o	1900	67.0	58.3	65.1	57.9

As noted by Bocalon *et al.* (2019), a clear difference of the detachment point between the peak and the trough is noticed in the Tab. 1, but the detachment happens further than the baseline, both at the peak and through, only for $4S$, $8S$ and $8M$ airfoils, in the specific configuration of a 2^o attack angle and at a Reynolds number of 1900. It was noticed a tendency to delay the detachment point with the reduction of the airfoils attack angle and with the increase of the Reynolds number, such a phenomenon also observed by Bocalon *et al.* (2019). Compared to the 2^o attack angle, the 8^o angle has a more clear difference of the detachment point between peak and trough, but it was not possible to generate such a conclusion when comparing different Reynolds numbers.

In absolute terms, considering a tolerance of $\pm 5.0\%$, the numerical results presented here corroborate the experimental results obtained by Bocalon *et al.* (2019) with a frequency of 46.7%. For a tolerance of $\pm 15\%$, the reliability of the numerical results rises to 93.3% when compared to visualizations of Bocalon *et al.* (2019). The 100% reliability is achieved with a tolerance of $\pm 17.0\%$. From the point of view only of the delay or anticipation of the detachment point, the numerical visualization identified the same relative behavior between the modified and baseline airfoils observed by Bocalon *et al.* (2019) with a frequency of $\pm 75.0\%$.

Based on the relationship between the detachment of the boundary layer and the lift coefficient presented by Johari *et al.* (2007), it is possible to conclude that the $4S$ airfoil performs a higher lift coefficient then the baseline one in the specific configuration of 2^o attack angle and at 1900 Reynolds number, which is consistent with the phenomenon observed by Bocalon *et al.* (2019) and also by Johari *et al.* (2007). Furthermore, in the same flow configuration, a performance improvement was also noted for the $8S$ and $8M$ airfoils compared to the baseline one. However, numerical evidence to identify which of the modified airfoils ($4S$, $8S$ or $8M$) provides the highest lift gain has not yet been obtained.

Therefore, in addition to the experimental results presented by Bocalon *et al.* (2019), for an angle and attack of 2^o and at 1900 Reynolds number, numerical evidence was produced suggesting lift gains by three modified airfoils: $4S$, $8S$ and $8M$. Aiming to quantify such gains, further works of post-processing are being developed with the same results produced by this study.

4. ACKNOWLEDGEMENTS

The authors are grateful to the Computational Support Center of Mechanical Engineering of the São Paulo State University (NACCEM-UNESP) and the Scientific Computing Center (NCC-GridUNESP), which provided the required infrastructure to perform this research.

This work has been possible in function of the São Paulo Research Foundation (FAPESP) grants, processes 2019/07947-0 (Regular Process) and 2020/02912-0 (Scientific Initiation).

5. REFERENCES

Barton, I.E., 1998. "Comparison of simple-and piso-type algorithms for transient flows". *International Journal for numerical methods in fluids*, Vol. 26, No. 4, pp. 459–483.

Bocalon, F.H.P., Amadeu, L., Coimbra, P.V.S. and Pantaleão, A.V., 2019. "Flow visualization in airfoil with leading edge protuberances applied to aerodynamics". *COBEM Uberlândia, MG, 25th Internetional Congress of Mechanical Engineering.*

Broadhead, B.L., Rearden, B.T., Hopper, C.M., Wagschal, J. and Parks, C.V., 2004. "Sensitivity-and uncertainty-based criticality safety validation techniques". *Nuclear science and engineering*, Vol. 146, No. 3, pp. 340–366.

Celik, I.B., Ghia, U., Roache, P.J. and Freitas, C.J., 2008. "Procedure for estimation and reporting of uncertainty due to discretization in cfd applications". *Journal of fluids Engineering-Transactions of the ASME*, Vol. 130, No. 7.

Chen, J.H., Li, S.S. and Nguyen, V.T., 2012. "The effect of leading edge protuberances on the performance of small aspect ratio foils". *15th International Symposium on Flow Visualization*.

Darwin, C., 1859. *On the Origin of Species by Means of Natural Selection, or The Preservation of Favoured Races in the Struggle for Life*.

Eça, L., Hoekstra, M. and Roache, P., 2007. "Verification of calculations: an overview of the 2nd lisbon workshop". In *18th AIAA Computational Fluid Dynamics Conference*. p. 4089.

Ferziger, J.H. and PERIĆ, M., 1996. "Further discussion of numerical errors in cfd". *International Journal for Numerical Methods in Fluids*, Vol. 23, No. 12, pp. 1263–1274.

Fish, F. and Battle, J.M., 1995. "Hydrodynamic design of the humpback whale flipper". *Journal of Morphology,225, 51-60*.

Hansen, K., Kelso, R., Dally, B. and Batill, S.M., 2009. "The effect of leading edge tubercle geometry on the performance of different airfoils". *ExHFT-7,Krakow, Poland*.

Hansen, K.L., Rostamzadeh, N., Kelso, R.M. and Dally, B.B., 2016. "Evolution of the streamwise vortices generated between leading edge tubercles". *Journal of Fluid Mechanics*, Vol. 788, pp. 730–766.

Issa, R.I., 1986. "Solution of the implicitly discretised fluid flow equations by operator-splitting". *Journal of computational physics*, Vol. 62, No. 1, pp. 40–65.

Johari, C., Henoch, D. and A., C.L., 2007. "Effects of leading-edge protuberances on airfoil performance". *AIAA J OURNAL Vol. 45, No. 11*.

Maliska, C.R., 2017. *Transferência de calor e mecânica dos fluidos computacional* . Grupo Gen-LTC.

Menter, F.R., 1994. "Two-equation eddy-viscosity turbulence models for engineering applications". *AIAA journal*, Vol. 32, No. 8, pp. 1598–1605.

Moukalled, F., Mangani, L. and Darwish, M., 2016. *The Finite Volume Method in Computational Fluid Dynamics*.

$OpenFOAM^{®}$, 2011. "Openfoam user guide". URL `https://www.openfoam.com/documentation/user-guide/`.

Patankar, S.V. and Spalding, D.B., 1983. "A calculation procedure for heat, mass and momentum transfer in three-dimensional parabolic flows". In *Numerical prediction of flow, heat transfer, turbulence and combustion*, Elsevier, pp. 54–73.

Paula, A.A., Padilha, B.R.M., Mattos, B.d.S. and Meneghini, J.R., 2016. "The airfoil thickness effect on wavy leading edge performance". *AIAA SciTech San Diego, California, USA 54th AIAA Aerospace Sciences Meeting*.

Perez Torro, R. and Kim, J.W., 2017. "A large-eddy simulation on a deep-stalled aerofoil with a wavy leading edge". *Journal of Fluid Mechanics*, Vol. 813, pp. 23–52.

Richardson, L.F., 1911. "Ix. the approximate arithmetical solution by finite differences of physical problems involving differential equations, with an application to the stresses in a masonry dam". *Philosophical Transactions of the Royal Society of London. Series A, Containing Papers of a Mathematical or Physical Character*, Vol. 210, No. 459-470, pp. 307–357.

Richardson, L.F. and Gaunt, J.A., 1927. "Viii. the deferred approach to the limit". *Philosophical Transactions of the Royal Society of London. Series A, containing papers of a mathematical or physical character*, Vol. 226, No. 636-646, pp. 299–361.

Roache, P.J., 1993. "A method for uniform reporting of grid refinement studies". *ASME-PUBLICATIONS-FED*, Vol. 158, pp. 109–109.

Rostamzadeh, N., Kelso, R.M. and Dally, B., 2017. "A numerical investigation into the effects of reynolds number on the flow mechanism induced by a tubercled leading edge". *Theoretical and Computational Fluid Dynamics*, Vol. 31, No. 1, pp. 1–32.

Van Nierop, E.A., Alben, S. and Brenner, M.P., 2008. "How bumps on whale flippers delay stall: an aerodynamic model". *Physical review letters*, Vol. 100, No. 5, p. 054502.

Versteeg, H.K. and Malalasekera, W., 2007. *An introduction to computational fluid dynamics: the finite volume method*.

Wei, Z., New, T. and Cui, Y., 2015. "An experimental study on flow separation control of hydrofoils with leading-edge tubercles at low reynolds number". *Ocean Engineering*, Vol. 108, pp. 336–349.

6. RESPONSIBILITY NOTICE

The authors are solely responsible for the printed material included in this paper.